

Basic research on determining optical properties of tissues *in vivo* by measuring diffuse reflectance with a charge-coupled device

PING SUN*, XIANPING CAO, RUNQIU YANG, FENGHUA XIE, JIAQI DING, FUQIANG ZHANG

Department of Physics, Beijing Normal University, Beijing Area Major Laboratory of Applied Optics, Beijing, 100875, P.R. China

*Corresponding author: pingsun@bnu.edu.cn

We measured the absorption coefficient and the reduced scattering coefficient of Intralipid solution and human forearm tissues *in vivo* by measuring diffuse reflectance with a charge-coupled device, examining the techniques involved. The experimental results indicate that the error is less than or equal to 8% using the diffusion theory, under the condition that the reduced scattering coefficient is one order of magnitude greater than the absorption coefficient. The stability and precision of optical property measurements are significantly improved by using the multistep iterative fitting method and using the ring-zone-constraint method to determine the diffuse reflectance center. The efficiency of reverse algorithm is greatly enhanced by selecting a one-dimensional array on the straight line crossing both the entry point and the diffusion center for fitting.

Keywords: diffusion theory, turbid media.

1. Introduction

Photodynamic therapy (PDT) has become a common therapeutic treatment in medicine with the rapid development of laser technology in recent years [1, 2]. For safe and effective implementation of PDT in clinical applications, accurate calculation of light dose is necessary. Two important optical parameters of human tissues for calculating the light dose are the absorption coefficient μ_a and the reduced scattering coefficient μ_s [3]. Moreover, these optical parameters provide information on tissue metabolism, pathological change, and especially cancer development [4]. Therefore, it is crucial to determine optical parameters *in vivo* by a safe, noninvasive, real-time, and accurate method. Now the primary method is first detecting the distribution of diffuse reflectance of light emitted from tissues, and then performing the reverse algorithm to determine the optical parameters [5–9]. The reverse algorithm is generally based on the diffusion theory [10–13]. Determination of optical properties of tissues by measuring diffuse reflectance has been accepted as a promising tool. However, it

is still necessary to pay more attention to the basic research on effective use of diffusion theory.

The oblique incidence method proposed by WANG *et al.* [14–16] is based on the two-source diffusion theory model of spatially resolved, steady-state diffuse reflectance [13]. In our previous work, we detected diffuse reflectance with optical fibers, and measured the absorption coefficient and reduced scattering coefficient of the Intralipid fat emulsion, *in vitro* tissue, and human forearm tissue [17, 18]. Studies demonstrated that this approach was feasible to be employed for measuring optical properties of tissues *in vivo*.

In this study, we used a charge-coupled device (CCD) to detect the distribution of diffuse reflectance of tissue, and investigated some basic questions involved, such as quantization of diffusion approximation theory, accuracy of measured optical parameters, effective reverse algorithm, determination of diffusion center and the processing method of diffuse reflectance raw data. Validity of the research results is tested on forearm tissue *in vivo*.

2. Methodology

2.1. Theory

The method to determine oblique-incidence diffuse reflectance is based on the steady-state diffusion theory with two sources [13]. As shown in Fig. 1, the distance from the photon source at $z = z_0$ to the extrapolated boundary is $z_0 + z_b$, and the distance

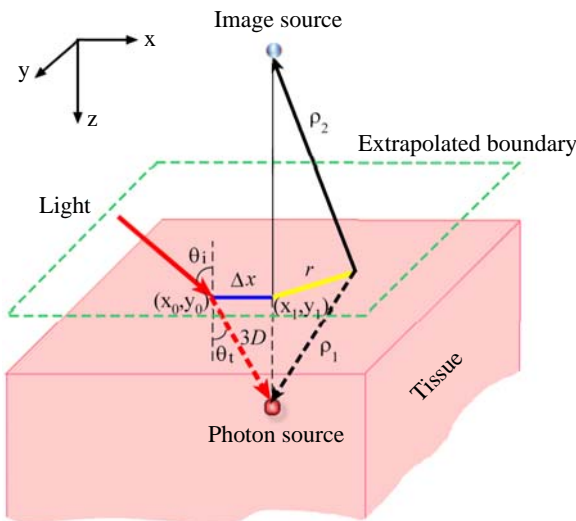


Fig. 1. A schematic diagram illustrating the isotropic point source, point source of mirror image, and extrapolated boundary.

from the point source of the mirror image to the extrapolated boundary is also $z_0 + z_b$. When a light beam is oblique to the surface of the biological tissue, the distance from the photon source along the direction of Snell's law of refraction to the light entry point is $3D$. D is the coefficient of diffusion, which is an optical parameter related to μ_a and μ'_s , $D = 1/[3(0.35\mu_a + \mu'_s)]$. Thus the equivalent point source relative to the light entry point has an offset in the direction of x , whose magnitude is $\Delta x = \sin \theta_t / (0.35\mu_a + \mu'_s)$ where θ_t is the refraction angle of light at the tissue–air interface. Given the incident angle of light and the refractive index of tissue, θ_t can be obtained from Snell's law. Thus the diffuse reflectance at the tissue surface can be obtained as [10, 13]:

$$R(r) = z_0 \left(\mu_{\text{eff}} + \frac{1}{\rho_1} \right) \frac{\exp(-\rho_1 \mu_{\text{eff}})}{4\pi\rho_1^2} + (z_0 + 2z_b) \left(\mu_{\text{eff}} + \frac{1}{\rho_2} \right) \frac{\exp(-\rho_2 \mu_{\text{eff}})}{4\pi\rho_2^2} \quad (1)$$

where $\rho_1 = [(z - z_0)^2 + r^2]^{1/2}$, $\rho_2 = [(z + z_0 + 2z_b)^2 + r^2]^{1/2}$, $z_0 = 3D \cos \theta_t$, $z_b = 2AD$ and μ_{eff} is an effective extinction coefficient related to μ_a and μ'_s , shown as: $\mu_{\text{eff}} = [3\mu_a(0.35\mu_a + \mu'_s)]^{1/2}$. A is related to the internal reflection and has an empirical value $A = (1 + r_i)/(1 - r_i)$, where $r_i = -1.440n_{\text{rel}}^{-2} + 0.710n_{\text{rel}}^{-1} + 0.668 + 0.0636n_{\text{rel}}$, and $n_{\text{rel}} = n_t/n_a$ is defined as relative index of the tissue–air interface.

When a nonlinear least-square fitting algorithm is performed in the distribution of diffuse reflectance, the effective extinction coefficient μ_{eff} can be obtained. If the offset value Δx is further calculated, then both μ_a and μ'_s can be obtained using the following equations:

$$\begin{cases} \mu_a = \frac{\mu_{\text{eff}}^2 \Delta x}{3 \sin \theta_t} \\ \mu'_s = \frac{\sin \theta_t}{\Delta x} - \frac{7\mu_{\text{eff}}^2 \Delta x}{60 \sin \theta_t} \end{cases} \quad (2)$$

2.2. Determination of the light entry point

Prior to collecting the distribution of light diffuse reflectance in the sample, the spatial coordinates of the entry point have to be determined. The sample was covered by a black film. A light beam irradiated the film surface from a particular angle, while a monochrome CCD camera captured the image. The digital format of the image is a two-dimensional matrix, with each element (a pixel) having its own coordinates and a gray value proportional to the light intensity. The pixel coordinate denotes the position of the pixel in the matrix, and is given by integers, represented by (i, j) . In this study, the center of the circular area which is outlined by pixels with average

light intensity is designated as the incident point. The average light intensity was calculated by the equation

$$\bar{I} = \frac{\sum_{i=1}^N \sum_{j=1}^N I_{ij}}{N}$$

where N is the number of total pixels in the image, and I_{ij} is the light intensity corresponding to the pixel coordinate (i, j) . The pixel coordinate (x_0, y_0) of the entry point was obtained by a weighted average of the light intensity

$$\left\{ \begin{array}{l} x_0 = \frac{\sum_{i=1}^{N'} I_{ij} i}{\sum_{i=1, j=1}^{N'} I_{ij}} \\ y_0 = \frac{\sum_{j=1}^{N'} I_{ij} j}{\sum_{i=1, j=1}^{N'} I_{ij}} \end{array} \right. \quad (3)$$

where N' is the number of pixels with light intensity greater than the average value \bar{I} .

2.3. Determination of diffusion center

From the diffusion equation (1), the light intensity distribution of diffuse reflectance is circularly symmetric. Enlightened by this symmetry we proposed a ring-zone-constraint method to determine the diffuse reflectance center. A ring zone outlined by two circular lines of pixels with equal light intensity was selected in the image; the center of the ring zone was designated as the diffusion center. Considering great CCD saturation close to the entry point, and a low signal-to-noise ratio far from the entry point, the ring zone should be confined to the appropriate intensity range. Figure 2 shows a suitable ring zone, where the diffusion center is located exactly in the center of the ring zone. Our program selected the range of the ring zone by obtaining minimal measurement errors for μ_a and μ'_s . For a brief description, the inner circle radius first remained constant, the measuring point was fitted to the following equation of a circle $(x - x_1)^2 + (y - y_1)^2 = R_2^2$, utilizing nonlinear least-square method. The outer circle radius R_2 was then determined with minimal errors of μ_a and μ'_s values. R_2 value was then fixed, the measuring point was fitted to the circle equation $(x - x_1)^2 + (y - y_1)^2 = R_1^2$ again by the nonlinear least-square method with minimal errors of μ_a and μ'_s values. Thus the inner circle radius R_1 was obtained. The pixel

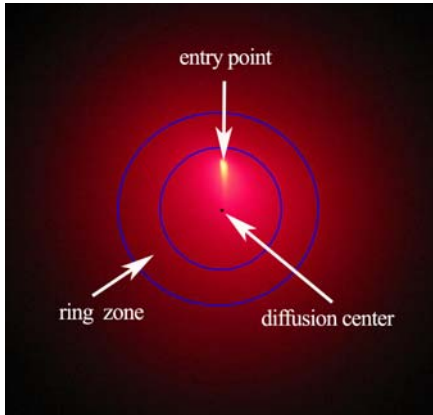


Fig. 2. A schematic diagram illustrating the ring zone, entry point and the diffusion center

coordinate of the center (x_1, y_1) , was chosen as the estimated diffusion center. As a result, the optimal area of the ring zone was outlined by two circles with radius R_2 and R_1 , respectively.

2.4. Selection of original data

The sample image captured with a 12-bit monochrome CCD camera possesses 10^6 data points. A one-dimensional curve fitting approach was applied for high efficiency. First, a straight line was drawn to cross both the entry point (x_0, y_0) and the diffusion center (x_1, y_1) , and the line equation is given below:

$$\frac{x - x_0}{y - y_0} = \frac{x - x_1}{y - y_1} \quad (4)$$

Points with set intervals on this line were then selected as original data points. The spline interpolation method was then implemented in these data points, and the pixel coordinate corresponding to the maximum intensity was determined to be the optimal diffusion center.

2.5. Calibration of pixel

The actual CCD pixel length K was determined through a calibration procedure. To determine K value, a black body with a 12-mm radius was used as a calibration piece. It was placed at the same height as the sample when its image was captured. The automatic identification of the calibration piece was implemented into our program, and the number of pixels M in the image was calculated. It is obvious that $K \approx \sqrt{\pi r^2 / M}$ when $M \rightarrow \infty$, where r is the radius of the calibration piece. In this study, when $M \geq 10^6$, the relative error of K is very small, as shown by $\Delta K / K \leq 0.1\%$.

2.6. Basic concept and flowchart of the program

The above techniques were executed using a Matlab program. The basic concept and flowcharts of the program are shown in Fig. 3.

Figure 3a is the flowchart for determining the entry point. The image data of the entry point was input; the position of the entry point was then obtained by Eq. (3) following calculation of the average light intensity \bar{I} .

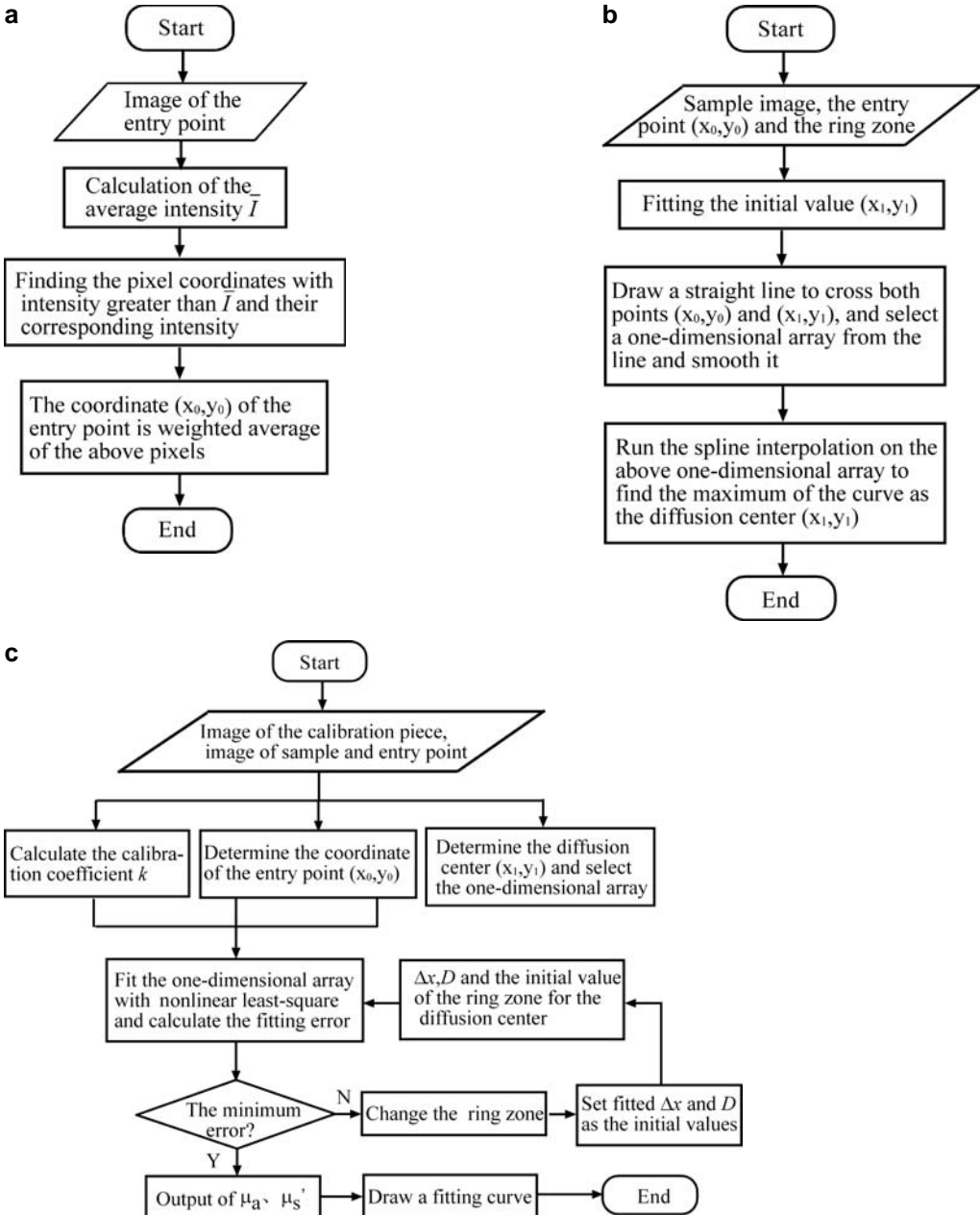


Fig. 3. Flowcharts for determining the entry point, the diffusion center and the main program. The entry point (a). The diffusion center (b). The main program (c).

Figure 3b is the flowchart for determining the diffusion center. The image data of the sample and the initial ring zone were input, and the initial value of the diffusion center was fitted. The one-dimensional array was then obtained from Eq. (4), and the diffusion center was determined by the one-dimensional array together with the entry point.

Figure 3c is the flowchart of the main program. First, the image of calibration piece, entry point and sample image data were input. Then the pixel length K , the spatial coordinates of entry point and the diffusion center were calculated. The one-dimensional array was also obtained, which would be further fitted. In this study, the multi-step iterative fitting method was used for multiple parameters fitting.

For a predefined ring zone, the total light intensity and Δx were first fixed, and the fitting algorithm was performed for D . Then Δx was fitted using the total light intensity and D . The total light intensity was further fitted using D and Δx . The above procedures were repeated until a minimum difference between the latest two fittings was obtained. If a minimum error cannot be obtained, then the initial ring zone has to be redefined. The above process was repeated until the error reached the minimum. Finally, μ_a and μ'_s values were calculated, and the fitting curve for diffusion was drawn out.

3. Experiment

The feasibility and accuracy of the proposed techniques in this study were examined with a similar experiment before being used for biological tissues. Intralipid, a fat emulsion, has been used as a standard agent for this purpose [19].

Intralipid solution (Sino-Swed Pharmaceutical Corp. Ltd.) and pure ink were used as additives. A set of liquid phantoms with different optical properties were obtained. Previous study indicated that the absorption of the Intralipid solution was primarily attributed to water, with a magnitude of 10^{-3} mm^{-1} [20, 21]. Thus it was considered as a purely scattering additive, mainly affecting μ'_s . Ink, an absorber, primarily influences μ_a . An Intralipid solution (10%) was diluted with deionized water to a serial of solutions with volume concentration C of 0.3%, 0.5%, 1.0%, 1.5%, 2%, 5% and 10%, respectively. These solutions were evenly dispersed with an ultrasonic apparatus and then used for measurement immediately.

3.1. Calibration of pixel

The image was captured with a 12-bit monochrome CCD camera (DH-SV1420FM, China Daheng Group, Inc.), with the resolution of 1392×1040 pixels, and pixel size of $4.65 \mu\text{m} \times 4.65 \mu\text{m}$. A lens with focus length of 8 cm was collocated on the CCD camera. A semiconductor laser (Beijing LASER OptoMechatronic Studio, Ltd.) was used, with a wavelength of 660 nm and continuous power output in a range of 0–20 mW. The experimental set-up is shown in Fig. 4. The collimated light beam was incident into the Intralipid solution after passing through a 1 mm aperture. The CCD

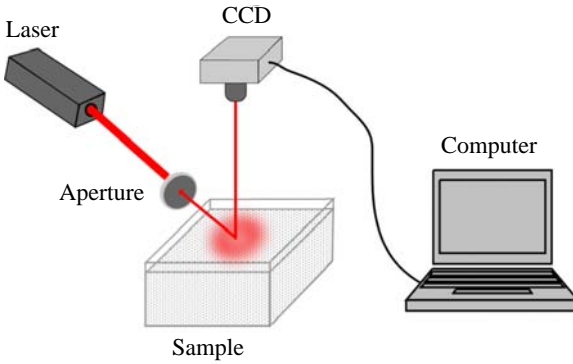


Fig. 4. A sketch diagram of the experimental setup.

camera detected light diffuse reflectance from the surface, and a computer software converted the image intensity into 0–4096 gray values.

The calibration piece was first placed at the same height of the Intralipid solution surface, and the calibration image was captured. A black film was placed on the sample solution surface, and the light entry point was captured. The black film was then removed and the light diffuse reflectance from the solution was captured. These three images were input to the program for fitting. Figure 5 shows the results measured from the Intralipid solutions at concentrations of 0.5% and 1%, where the y axis represents the normalized light intensity.

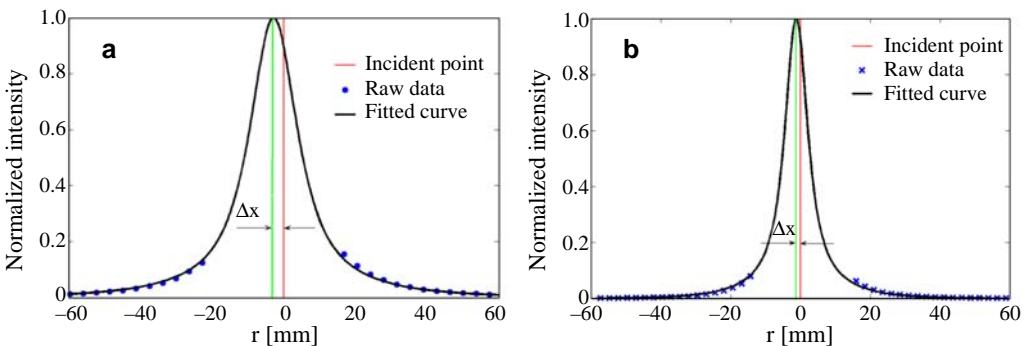


Fig. 5. The measurement results of the Intralipid solutions at concentrations of 0.5% (a) and 1% (b).

The measured values of Intralipid solutions at different concentrations are provided in Tab. 1. A refractive index of 1.35 was used for the Intralipid solution when the fitting method was performed. The experimental results are similar to those obtained in our previous study, but have higher accuracy [18].

One assumption for the diffusion approximation theory is $\mu'_s/\mu_a \gg 1$, which was examined in our study. Setting $\mu'_s = 0.5479 \text{ mm}^{-1}$, μ_a value was varied by adding ink to Intralipid solutions at different concentrations, and the error y_{error} of μ'_s was

Table 1. Optical properties of different Intralipid solutions.

C [%]	μ_a [mm^{-1}]	μ'_s [mm^{-1}]	Δx [mm]	μ_{eff} [mm^{-1}]
10	0.0067	8.9970	0.0597	0.2846
5	0.0055	4.8702	0.1104	0.2094
2	0.0072	2.1807	0.2420	0.1401
1.5	0.0067	1.5067	0.3162	0.1166
1	0.0057	1.0847	0.4909	0.0989
0.5	0.0062	0.4682	1.1626	0.0651
0.3	0.0056	0.3041	1.7922	0.0526

Table 2. The influence of μ_a on the accuracy of μ'_s measurement.

μ_a [mm^{-1}]	μ'_s [mm^{-1}]	μ'_s/μ_a	y_{error} [%]
0.0062	0.5479	88.37	0.00
0.0202	0.5237	25.93	4.42
0.0460	0.5873	12.77	7.19
0.1381	0.4860	3.52	11.30
0.1570	0.4852	3.09	11.44
0.1955	0.4771	2.44	12.92
0.2642	0.4057	1.54	25.95

measured. Table 2 shows the experimental results. Again the refractive index is 1.35 when the fitting method was applied.

3.2. Optical properties of the human forearm tissue

The refractive index of the human body was set as $n = 1.39$ for the fitting, based on a previous study on human skin [22]. The μ_a and μ'_s values of the forearms of 12 Chinese volunteers (5 females and 7 males, aged 20–45 years) were measured. The experimental set-up is shown in Fig. 4. Volunteers placed their forearms on the platform while keeping muscles in a relaxed state. The smooth part of forearms



Fig. 6. Burn scars on volunteer No. 4.

T a b l e 3. Optical properties of human forearms.

No.	μ_a [mm ⁻¹]	μ'_s [mm ⁻¹]	No.	μ_a [mm ⁻¹]	μ'_s [mm ⁻¹]
1a	0.0166	1.5720	5	0.0387	0.8053
1b	0.0128	1.5630	6	0.0859	0.3237
2a	0.0831	0.4092	7	0.0581	1.0280
2b	0.0637	0.5899	8	0.0476	0.3243
3a	0.0350	0.7903	9	0.0146	0.8063
3b	0.0609	0.7856	10	0.0463	0.4924
4a	0.0345	0.6496	11	0.0563	0.3928
4b	0.0695	0.3514	12	0.0463	0.4924

* a and b denote the different positions of the same volunteer.

was measured. Some volunteers had burn scars or moles on their forearms. The burn scars on volunteer No. 4 were marked by arrows in Fig. 6. Table 3 shows the experimental results.

4. Results and discussion

During the experiment, we observed that the lower the Intralipid solution concentration, the greater the distance between the diffusion center and the entry point as shown in Fig. 5. When the concentration is greater than 1%, a slight difference is observed, which agrees with the experimental results in Tab. 1. When the concentration is 1%, Δx is approximately 0.5 mm, and it is difficult to distinguish between these two by naked eyes. As shown in Tab. 1, the reduced scattering coefficient of the Intralipid solution is bigger when the concentration is higher, which indicates that the mean free path is shorter when the light travels in the solution. Thus the light would be scattered within a short distance after entering the solution.

Light absorption from Intralipid solutions at 660 nm is close to that of water. From the study of HALE and QUERRY, the absorption coefficient of water at 660 nm is about 0.002 mm⁻¹ [23]. The μ_a values in different Intralipid solutions in Tab. 1 are of the same order of magnitude as those from Hale's study [23]. Variance in water quality could account for the slight difference. Due to the different particle sizes and constituents in Intralipid solutions, the optical properties vary in different studies [19–21, 24–26]. STAVEREN *et al.* proposed two empirical equations for the scattering coefficient μ_s and the anisotropic factor g in Intralipid 10% solution [19], which are $\mu_s(\lambda) = 0.016\lambda^{-2.4}$ and $g = 1.1 - 0.58\lambda$. When $\lambda = 660$ nm, $g = 0.72$ and $\mu_s = 43.37$ mm⁻¹ in Intralipid 10% solution. Figure 7 shows the measurement, fitting and estimated values of μ_s and μ'_s , where the discrete diamonds represent the measuring results of μ'_s from Tab. 1. Line I was obtained using the straight-line fitting method. Line II was obtained by applying line I data to the equation $\mu_s = \mu'_s/(1 - g)$. Line III was obtained by estimating the corresponding values of μ_s in different concentrations

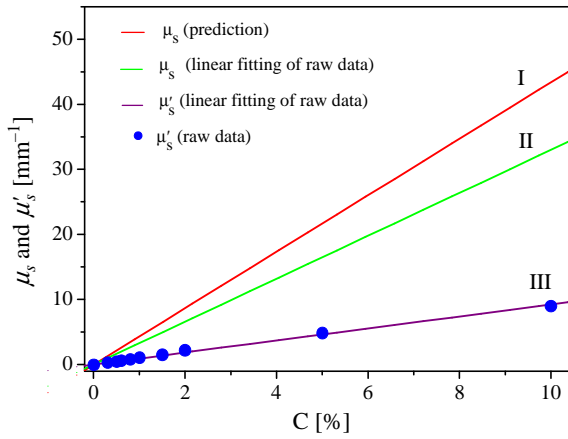


Fig. 7. The measurement, fitting and estimated values of μ_s and μ'_s .

with the equation given by STAVEREN *et al.* [19]. Comparing lines II and III, we find that the difference between measured values and estimated values increases as the solution concentration increases. For example, when $C = 0.5\%$, the measured value is 1.3086 mm^{-1} and the estimated value is 1.7213 mm^{-1} , with a difference of $\sim 0.4 \text{ mm}^{-1}$. However, when $C = 10\%$, the measured value is 32.97 mm^{-1} and the estimated value $\mu_s = 43.37 \text{ mm}^{-1}$, with a bigger difference of $\sim 10.4 \text{ mm}^{-1}$. The measured values in current work are very close to those from our previous study (33.21 mm^{-1}) [18], as well as studies of MOES *et al.* (38.6 mm^{-1}) [25] and CHEN *et al.* (30 mm^{-1}) [26].

The data in Tab. 2 was fitted for evaluating measurement error of μ'_s caused by increasing μ_a values, by $y_{\text{error}} = 742\exp(-\mu'_s/0.388\mu_a) + 13.1\exp(-\mu'_s/24.4\mu_a) - 0.315$, where y_{error} is the relative error subject to the exponential decay when μ'_s/μ_a changes. Figure 8 shows that when $\mu'_s/\mu_a < 10$, the measurement error of μ'_s increases rapidly,

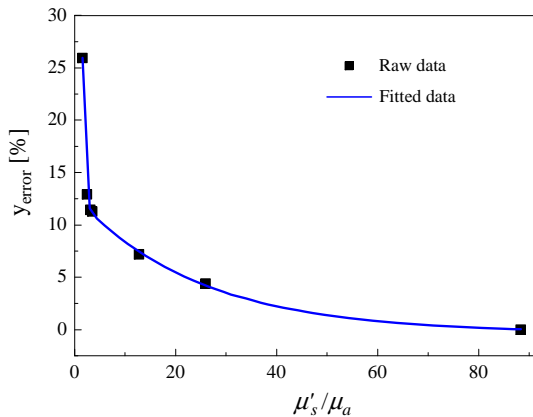


Fig. 8. The influence of the absorption coefficient on the reduced scattering coefficient.

while when $\mu'_s/\mu_a \geq 10$, the error is less than or equal to 8%. Based on that, we conclude that the measurement error is not greater than 8% if μ'_s is one order of magnitude greater than μ_a .

From Table 3, we can see that μ_a value ranges from 0.01 to 0.09, and μ'_s value is 0.3 to 1.1 in our studies. There is a slight difference in the values among different individuals. Optical parameters of human skins reported in different studies are different, which could be due to the different measure methods and different subjects [3, 27–29]. However, the statistics show that μ_a of human skins is in the range of 10^{-2} – 10^{-1} mm⁻¹, and μ'_s is in the range of 10^{-1} – 1 mm⁻¹. Overall, our results are consistent with the results obtained by others.

Different positions on the forearms of volunteers No. 1–4 were measured. A slight difference was found between different positions for a normal skin, for example, datasets *a* and *b* from volunteer No. 1 as well as those from volunteer No. 2. However, for special positions such as a scar or mole, measured results are different from those of the normal skin, which can be seen in the two datasets from volunteers No. 3 and 4. Although the μ'_s of the normal tissue (*a*) and a mole (*b*) are close for volunteer No. 3, the μ_a of the normal tissue is greater than that of the mole. The results from volunteer No. 4 were obtained from the normal tissue (*a*) and a burn scar (*b*). We found that μ_a of the burn scar is greater than that of the normal tissue, whereas μ'_s of the burn scar is less than that of the normal tissue. YANG *et al.* proposed that benign birthmarks or scars would not influence scattering properties [28], which however is not true in our study.

In this study, we determined μ_a and μ'_s indirectly. The measurement errors come from the direct measurement of Δx and μ_{eff} . When $\mu'_s/\mu_a \gg 1$, the relative error of μ_a is shown as

$$\frac{\Delta\mu_a}{\mu_a} = \frac{\Delta(\Delta x)}{\Delta x} + 2 \frac{\Delta\mu_{\text{eff}}}{\mu_{\text{eff}}}$$

derived from Eq. (2), and the relative error of μ'_s is equal to the relative error of Δx . Under our experimental conditions, the relative error of Δx is 5% (mainly depending on the CCD resolution), and the relative error of μ_{eff} is 0.03% (mainly depending on the light intensity errors detected by CCD). Compared with the former, the latter is negligible. Statistical error can occur when the fitting method is applied to data (the difference between the fit point and measuring point divided by the absolute value of fit point). Using the approach proposed in this study a statistical error not greater than 0.0001% was obtained, which is negligible compared with the relative error of Δx and μ_{eff} . Considering Δx and μ_{eff} were obtained using the iterative fitting method, Δx and μ_{eff} are close to the actual values, and the error would always be less than the initial value. Therefore, the measurement error of μ_a and μ'_s in this study is less than 5%.

5. Conclusions

Based on the diffusion approximation theory, the absorption coefficient and the reduced scattering coefficient of Intralipid solution and human forearm tissues were determined. The results indicate that the measurement error is not greater than 8% if the scattering coefficient is one order of magnitude greater than the absorption coefficient. A ring zone was used to determine the diffuse reflectance center, and the absorption coefficient and reduced scattering coefficient were obtained through a reverse multistep iterative fitting. A one-dimensional array was selected on the straight line crossing both the entry point and the diffusion center, which was used for the reverse fitting method. The stability and precision of optical properties were significantly improved, and the efficiency of reverse fitting algorithm was greatly enhanced by our method. The relative error of the absorption coefficient and the reduced scattering coefficient are less than 5% in this study. The distribution of diffused light on the sample was collected by a CCD camera, which is easy to use and suitable for many other applications. The automatic fitting algorithm in Matlab, independently developed by the authors, has high efficiency and many practical applications. The techniques of this study are suitable for all skin tissues although only forearm tissues *in vivo* were measured. The results presented herein can be used as guidance and offer important technical information for applications of the diffusion theory.

Acknowledgements – This research is supported by Beijing Natural Science Foundation for funds (grant number: 4102031). We also express our gratitude to all the volunteers who participated in this study.

References

- [1] WILSON B.C., PATTERSON M.S., *The physics, biophysics and technology of photodynamic therapy*, *Physics in Medicine and Biology* **53**(9), 2008, pp. R61–R109.
- [2] WANG H.-W., ZHU T.C., PUTT M.E., SOLONENKO M., METZ J., DIMOFTE A., MILES J., FRAKER D.L., GLATSTEIN E., HAHN S.M., YODH A.G., *Broadband reflectance measurements of light penetration, blood oxygenation, hemoglobin concentration, and drug concentration in human intraperitoneal tissues before and after photodynamic therapy*, *Journal of Biomedical Optics* **10**(1), 2005, p. 014004.
- [3] BASHKATOV A.N., GENINA E.A., KOCHUBEY V.I., TUCHIN V.V., *Optical properties of human skin, subcutaneous and mucous tissues in the wavelength range from 400 to 2000 nm*, *Journal of Physics D: Applied Physics* **38**(15), 2005, pp. 2543–2555.
- [4] DURDURAN T., CHO E., CULVER J.P., ZUBKOV L., HOLBOKE M.J., GIAMMARCO J., CHANCE B., YODH A.G., *Bulk optical properties of healthy female breast tissue*, *Physics in Medicine and Biology* **47**(16), 2002, pp. 2847–2861.
- [5] KIENLE A., LILGE L., PATTERSON M.S., HIBST R., STEINER R., WILSON B.C., *Spatially resolved absolute diffuse reflectance measurements for noninvasive determination of the optical scattering and absorption coefficients of biological tissue*, *Applied Optics* **35**(13), 1996, pp. 2304–2314.

- [6] DIMOFTE A., FINLAY J.C., ZHU T.C., *A method for determination of the absorption and scattering properties interstitially in turbid media*, *Physics in Medicine and Biology* **50**(10), 2005, pp. 2291–2311.
- [7] BARGO P.R., PRAHL S.A., GOODELL T.T., SLEVEN R.A., KOVAL G., BLAIR G., JACQUES S.L., *In vivo determination of optical properties of normal and tumor tissue with white light reflectance and an empirical light transport model during endoscopy*, *Journal of Biomedical Optics* **10**(3), 2005, p. 034018.
- [8] TSENG S.-H., GRANT A., DURKIN A.J., *In vivo determination of skin near-infrared optical properties using diffuse optical spectroscopy*, *Journal of Biomedical Optics* **13**(1), 2008, p. 014016.
- [9] YANG H.Q., XIE S.S., LI H., LU Z.K., *Determination of human skin optical properties in vivo from reflectance spectroscopic measurements*, *Chinese Optics Letters* **5**(3), 2007, pp. 181–183.
- [10] GROENHUIS R.A.J., FERWERDA H.A., BOSCH J.J.T., *Scattering and absorption of turbid materials determined from reflection measurements. 1: Theory*, *Applied Optics* **22**(16), 1983, pp. 2456–2462.
- [11] GROENHUIS R.A.J., BOSCH J.J.T., FERWERDA H.A., *Scattering and absorption of turbid materials determined from reflection measurements. 2: Measuring method and calibration*, *Applied Optics* **22**(16), 1983, pp. 2463–2467.
- [12] HIELSCHER A.H., JACQUES S.L., WANG L., TITTEL F.K., *The influence of boundary conditions on the accuracy of diffusion theory in time-resolved reflectance spectroscopy of biological tissues*, *Physics in Medicine and Biology* **40**(11), 1995, pp. 1957–1975.
- [13] FARRELL T.J., PATTERSON M.S., WILSON B., *A diffusion theory model of spatially resolved, steady-state diffuse reflectance for the noninvasive determination of tissue optical properties in vivo*, *Medical Physics* **19**(4), 1992, pp. 879–888.
- [14] WANG L., JACQUES S.L., *Use of a laser beam with an oblique angle of incidence to measure the reduced scattering coefficient of a turbid medium*, *Applied Optics* **34**(13), 1995, pp. 2362–2366.
- [15] LIN S.-P., WANG L., JACQUES S.L., TITTEL F.K., *Measurement of tissue optical properties by the use of oblique-incidence optical fiber reflectometry*, *Applied Optics* **36**(1), 1997, pp. 136–143.
- [16] MARQUEZ G., WANG L.V., LIN S.-P., SCHWARTZ J.A., THOMSEN S.L., *Anisotropy in the absorption and scattering spectra of chicken breast tissue*, *Applied Optics* **37**(4), 1998, pp. 798–804.
- [17] SUN P., WANG Y., MO X.L., XIE J.H., *Noninvasive determination of absorption coefficient and reduced scattering coefficient of human skin tissues in vivo with oblique-incidence reflectometry*, *Chinese Optics Letters* **6**(12), 2008, pp. 932–934.
- [18] SUN P., WANG Y., *Measurements of optical parameters of phantom solution and bulk animal tissues in vitro at 650 nm*, *Optics and Laser Technology* **42**(1), 2010, pp. 1–7.
- [19] VAN STAVEREN H.J., MOES C.J.M., VAN MARIE J., PRAHL S.A., VAN GEMERT M.J.C., *Light scattering in Intralipid-10% in the wavelength range of 400–1100 nm*, *Applied Optics* **30**(31), 1991, pp. 4507–4514.
- [20] POGUE B.W., WHITE E.A., ÖSTERBERG U.L., PAULSEN K.D., *Absorbance of opaque microstructures in optically diffuse media*, *Applied Optics* **40**(25), 2001, pp. 4616–4621.
- [21] FLOCK S.T., JACQUES S.L., WILSON B.C., STAR W.M., VAN GEMERT M.J.C., *Optical properties of Intralipid: A phantom medium for light propagation studies*, *Lasers in Surgery Medicine* **12**(5), 1992, pp. 510–519.
- [22] DING H.F., LU J.Q., WOODEN W.A., KRAGEL P.J., HU X.-H., *Refractive indices of human skin tissues at eight wavelengths and estimated dispersion relations between 300 and 1600 nm*, *Physics in Medicine and Biology* **51**(6), 2006, pp. 1479–1489.
- [23] HALE G.M., QUERRY M.R., *Optical constants of water in the 200-nm to 200- μ m wavelength region*, *Applied Optics* **12**(3), 1973, pp. 555–563.
- [24] DRIVER I., FEATHER J.W., KING P.R., DAWSON J.B., *The optical properties of aqueous suspensions of Intralipid, a fat emulsion*, *Physics in Medicine and Biology* **34**(12), 1989, pp. 1927–1930.
- [25] MOES C.J.M., VAN GEMERT M.J.C., STAR W.M., MARIJNISSEN J.P.A., PRAHL S.A., *Measurements and calculations of the energy fluence rate in a scattering and absorbing phantom at 633 nm*, *Applied Optics* **28**(12), 1989, pp. 2292–2296.

- [26] CHEN C., LU J.Q., DING H.F., JACOBS K.M., DU Y., HU X.-H., *A primary method for determination of optical parameters of turbid samples and application to Intralipid between 550 and 1630 nm*, Optics Express **14**(16), 2006, pp. 7420–7435.
- [27] DOORBOS R.M.P., LANG R., AALDERS M.C., CROSS F.W., STERENBORG H.J.C.M., *The determination of in vivo human tissue optical properties and absolute chromophore concentrations using spatially resolved steady-state diffuse reflectance spectroscopy*, Physics in Medicine and Biology **44**(4), 1999, pp. 967–981.
- [28] TROY T.L., THENNADIL S.N., *Optical properties of human skin in the near infrared wavelength range of 1000 to 2200 nm*, Journal of Biomedical Optics **6**(2), 2001, pp. 167–176.
- [29] ZONIOS G., DIMOU A., *Light scattering spectroscopy of human skin in vivo*, Optics Express **17**(3), 2009, pp. 1256–1267.

*Received November 12, 2010
in revised form February 18, 2011*